Chapter 6

Forecasting the geoeffectiveness of CMEs using Artificial Neural Network and forward modeling

6.1 Introduction

Coronal Mass Ejections (CMEs) are sudden energetic outbursts of a huge amount of plasma materials from the solar atmosphere into the heliosphere. These plasma materials often carry strong magnetic fields embedded in them (Chen, 2011; Webb and Howard, 2012). The space weather conditions in near-Earth space are predominantly governed by these energetic events from the Sun when they are directed towards the Earth. The interactions between these plasma materials and the embedded magnetic fields with the magnetosphere and upper atmosphere of Earth lead to consequences that range from the occurrences of spectacular auroras in polar regions to the severe geomagnetic storms causing damage to space-based assets like communication satellites, GPS systems, health hazards of astronauts, disturbances in aviation operations, and even power grid failure to name a few (Gopalswamy, 2022). Other than understanding the physical processes

behind the origin and evolution of CMEs and their propagation through interplanetary space, it is an urgent need of our increasingly space-based technology-dependent society to develop reliable and adequate space-weather forecasting capabilities to predict the timing and intensity of a possible geomagnetic storm well in advance with reasonable accuracy.

In the context of forecasting the geoeffectiveness of the CMEs, the two most important questions to be answered are, when will a CME arrive in the near-Earth space, and how much impact it will create. There have been numerous important studies on forecasting the transition time (TT) of a CME from the Sun to near-Earth space (Vourlidas et al., 2019). Riley et al. (2018) reported a comparative analysis of 32 distinct models (forecasts submitted to the Community Coordinated Modeling Center (CCMC)) for forecasting the arrival times of CMEs, the mean errors in the forecasts of these models are around ± 10 hours with standard deviations of around 20 hours. Although the arrival time of a CME is an important parameter for space weather forecasts, it does not indicate the severity of the geomagnetic storm (as measured by the Dst index). In that aspect, knowing the value of the southward magnetic field of the CME is crucial (Sarkar et al., 2020; Vourlidas et al., 2019). A model that can simultaneously and adequately predict the transition time of a CME from Sun to Earth and the Dst index of the geomagnetic storm to be caused by the CME can be a highly useful tool in space weather forecast research.

In recent times, there has been a significant rise in the use of Machine Learning techniques in the study and forecast of space weather due to the abundance of available observed data for efficient training of these algorithms. Sudar et al. (2016) used the initial space speed and the source locations of 153 CMEs as input parameters of an Artificial Neural Network (ANNs) and predicted the arrival times with an average error of ~ 12 h. Liu et al. (2018) utilized a Support Vector Machine (SVM) on a sample of 182 CMEs which showed impressive forecast capability with a Mean Absolute Error (MAE) of 5.9 h. More recently, Minta et al. (2023) used the solar wind and CME speeds as inputs to a

CFNN (Cascade Forward Neural Network) that gave a MAE of 7.3 h. ANNs have also been utilized in short-term forecasts of the intensity of geomagnetic storms in terms of the Dst index with a limited time window of a few hours (Abduallah et al., 2022; Bala and Reiff, 2012; Lazzús et al., 2017).

It is obvious that the initial parameters of the CMEs during their onset in the solar atmosphere play a critical role in having the maximum time window for the forecast of their transit time and geoeffectiveness. In this context, the forward modelling technique of the Graduated Cylindrical Shell (GCS, Thernisien et al. (2009)) model has been a reliable tool in probing the features of the flux rope structure from the coronagraph observations. Recently, it has been shown that the deprojected 3D speed of the CMEs as given by the GCS model, when used with the empirical model of CME arrival time, provides much better forecasts of CME transit times (Gopalswamy et al., 2005, 2013; Suresh et al., 2022).

One major advantage of the ANN algorithm is that, once trained on an already available dataset, it works reasonably well in predicting the values of desired parameters through regression or in performing the classification of events (Emmert-Streib et al., 2020). This is achieved by approximating mathematical relationships between the output and input variables through statistical analysis and optimization of the model parameters even in the cases when the exact physics-based reasoning behind these phenomena is not completely understood. Hence, in this work, we use the GCS model parameters of the fitted flux rope to a set of geoeffective CMEs as the inputs to an ANN in order to forecast the transit time of the CMEs and the hourly averaged peak Dst index of the corresponding geomagnetic storms.

6.2 Data and Method

To analyse the 3D evolution of the magnetic flux rope of a CME using the GCS model, multiview point coronagraphic observations of the events are required. The LASCO

instrument onboard the SOHO spacecraft has been taking coronagraph observations of the Sun since 1996. However, it is only after the launch of the twin STEREO spacecraft in 2007, that simultaneous multiview point observations of the CMEs are available. To create the dataset of the geoeffective CMEs, we used the near-Earth ICME list compiled and updated by Richardson and Cane (2010). The catalog (hosted at: https://izw1.caltech.edu/ACE/ASC/DATA/level3/icmetable2.htm) provides relevant information regarding the timing and intensity of the geomagnetic storms, the arrival time and speed of the corresponding near-Earth ICMEs, and about their possible near-Sun counterparts (Richardson and Cane, 2024). We selected the geomagnetic storms and the associated CME events for cycle 24 and the rising phase of cycle 25. Further, we impose the following criteria to refine the selection of events: (i) the geomagnetic storms must have a minimum Dst index value of -20 nT or lesser, (ii) the associated CME must be simultaneously and clearly visible in white light coronagraph images from at least two viewpoints among the three of COR2 FOV in SECCHI/STEREO A, and STEREO B, and C3 FOV of SOHO/LASCO spacecraft for better fitting of the flux rope. (iii) The CMEs must be present in at least three consecutive frames in COR2 A/B and C3 FOV.

Following the above-mentioned criteria, we finally selected a set of 67 events to perform our analysis. The 3D flux rope structure as assumed in the GCS model, resembles a hollow croissant-like shape with a torus-like front and conical legs joining each other at the centre of the Sun (Thernisien, 2011; Thernisien et al., 2009). The model provides six parameters for fitting of the flux rope structure to a CME, namely, (i) the height of the leading edge of the CME (h), (ii) latitude (θ), (iii) longitude (ϕ), (iv) half angle (α), (v) aspect ratio (κ), and (vi) tilt angle (γ). We utilize the GCS model implemented in Python for the fitting of the flux ropes (Forstner, 2024; Freiherr von Forstner, 2021). Once, the flux rope is fitted to a CME by adjusting these parameters, the evolution of the CME is tracked by varying the height of the flux rope considering the self-similar expansion of the flux rope

structure. The true speed of the CME (V_{GCS}) is finally calculated from the slope of the fitted straight line on the height-time data obtained following the above procedure (see Suresh et al. (2022), Majumdar et al. (2020) for more details regarding the same).

Here, we discuss the architecture of the Neural Network deployed for the work. ANNs are layered structures of 'cells' or 'neurons' connected with each other through weights that transform input parameters into output parameters. It can consist of multiple hidden layers in between the input and output layers having multiple numbers of neurons required for optimal performance of the network (Abiodun et al., 2018). The training of the algorithm is achieved by optimization of the loss function through the updation of the weights. Each connection consists of a bias and an activation function for determining the active state of the corresponding neuron. In this study, A fully connected feed-forward dense Neural Network was used with four hidden layers in between the input and the output layers. As we use the GCS parameters (the true speed, and the parameters (ii) to (vi) as mentioned above) as the inputs to the ANN, the input layer consists of six neurons and the output layer gives the value of the predicted Dst index and the transit time of the CME. The number of neurons in the four hidden layers is (8,6,4,2) respectively for the optimum performance. In all hidden layers, we use the Rectified Linear Unit (ReLU) activation function and in the output layer we use the Linear activation function, as this combination is considered to be most suitable for the type of regression problem we aim to perform in this work (Agarap, 2018; Apicella et al., 2021; Jagtap and Karniadakis, 2022). In case of the loss function for training the algorithm, we used the mean squared error (mse) calculated from the predicted and the observed values, and for the updation of the weights and biases of the connections, we utilise the ADAM optimiser, which is considered to be oe of the most time efficient optimizers of the present time (Kingma and Ba, 2014). Here, we would like to mention, that although the model architecture of the networks is the same, we use two different single-output networks for forecasting the CME transit time and the Dst index instead of a

Fig. 6.1 An example of the fitted flux rope structure (colored in blue) by using GCS model on the Halo CME event of 28 September 2012, 00:12 UT as observed from three different vantage points from COR2 FOV of STEREO B, C3 FOV of SOHO/LASCO, and COR2 FOV of STEREO A spacecraft respectively. For the calculation of the GCS parameters we utilize the GCS model implemented in Python (Forstner, 2024; Freiherr von Forstner, 2021). (available at: https://github.com/johan12345/gcs_python)

Table 6.1 A sample of the GCS parameters of a subset of 20 CME events from the selected dataset along with the time and intensity corresponding geomagnetic storm. The transit time (TT) is calculated from the time difference between the LASCO CME onset time (cloumn-1) and the geomagnetic disturbance time (column-8). For more details regarding the selected events, please refer to the catalog (Richardson and Cane, 2024) maintained by Richardson and Cane (2010)

LASCO CME Y/M/D (UT)	Half Angle (α) (deg)	κ	Latitude (θ) (deg)	Longitude (ϕ) (deg)	Tilt (γ) (deg)	V_{GCS} (km/s)	Disturbance Y/M/D (UT)	Dst (nT)	TT (hrs)
2010/04/03 1033	16.2	0.4	-24.5	7.5	-8.27	768.08	2010/04/05 0826	-81	45.88
2010/04/08 0454	14.89	0.37	-4.43	6.5	3	423.16	2010/04/11 1304	-67	80.17
2010/05/24 1406	22.89	0.52	0.92	16.88	-16.22	645.67	2010/05/28 0258	-80	84.87
2010/08/01 0845	20.89	0.73	20.2	330.5	-70	1541.23	2010/08/03 1741	-74	56.93
2011/02/15 0236	23.66	0.65	-5.27	3.1	42	710.83	2011/02/18 0130	-32	70.9
2011/03/03 0548	13.05	0.3	-22.04	6	19.29	393.65	2011/03/06 0331	-27	69.72
2011/06/02 0745	25.3	0.31	-2.75	7.5	-25.86	891.05	2011/06/04 2045	-45	61
2011/08/04 0412	65.1	0.71	23.88	31.88	-71.5	1356.21	2011/08/05 1751	-115	37.65
2011/09/06 2305	38.23	0.58	28.03	28.38	-83.2	552.85	2011/09/09 1242	-75	61.62
2011/09/19 0600	41.2	0.39	27.55	309.38	-72.55	704.65	2011/09/22 0300	-29	69
2011/09/24 1248	52.9	0.79	9.02	310.75	-73.55	1926	2011/09/26 1234	-118	47.77
2011/10/22 0005	73.35	0.62	50.27	30.75	-71.41	747.69	2011/10/24 1831	-147	66.43
2011/10/26 1000	10.15	0.45	12.61	30.88	-55.1	435.22	2011/10/30 1001	-29	96.02
2011/10/27 1200	24.75	0.34	35.82	311.63	-83.57	542.41	2011/11/01 0907	-66	117.12
2011/11/26 0700	29.92	0.86	22.96	35.64	-65.56	1064.63	2011/11/28 2150	-25	62.83
2012/01/19 1436	45.6	0.73	45.92	352.5	64.76	1176.04	2012/01/22 0611	-71	63.58
2012/02/24 0225	53.5	0.24	26.39	346.25	-84.57	891.02	2012/02/26 2139	-57	67.23
2012/03/04 1100	22.05	0.38	22.63	313.13	-65.1	947.49	2012/03/06 0800	-23	45
2012/03/07 0024	66.3	0.87	33.06	322.5	-73.46	2469.69	2012/03/08 1103	-145	34.65

single dual-output network. This is done to improve the optimization of the loss function, and time efficiency, resulting in better and quicker training of the networks, hence yielding a better forecast capability.

6.3 Results and Discussions

The Figure 6.1 shows the typical structure of the magnetic flux rope (blue mesh) fitted on the Halo CME event of 28 September 2012, 00:12 UT using the GCS model on the simultaneous observations (running difference images) from the STEREO and SOHO spacecrafts. We present the fitted GCS parameters for a subset of 20 CMEs in the Table 6.1 along with the calculated transit time (TT) of the CMEs and the peak of the Dst index during the associated geomagnetic storms. Column 1 of the table shows the CME onset time and column 8 notes the commencement time of the geomagnetic disturbance, i.e. the arrival of the CME in near-Earth space. For further details regarding these quantities, refer to the catalog (Richardson and Cane, 2024) maintained by Richardson and Cane (2010). The transit times are calculated from the time difference between the CME onset time (column 1) and the commencement time of the geomagnetic disturbance (column 8).

To validate our calculation of the CME ture speed, we compare the 3D speeds (V_{GCS}) with their 2D linear speeds (or the projected speeds of the CMEs on the plane of the sky) as available in the CDAW catalogue (Gopalswamy et al., 2009). In Figure 6.2a we plot the true speed with the 2D speed. The solid line indicates the region where these two speeds are similar. The plot shows that a significant portion of the CMEs have a true speed higher than the 2D speed. However, for many of the fast CMEs, the 2D speed is higher. This result is similar to what was found by Majumdar et al. (2020). The possible reason behind the projected 2D speed being higher than the true speed, can be due to the higher speed of lateral expansion of the CMEs than their radial speed of forward propagation (Gopalswamy et al., 2009; Shen et al., 2013). The Figure 6.2b shows the plot of the transit

times of the CMEs from the Sun to Earth at 1 AU with their respective true speeds. The time taken by the selected CMEs are within a range of around 35-120 hrs, and on average the transit time decreases with the increase in the CME speed, although the relationship between these quantities does not seem to be completely a linear one.

In the Figure 6.3a, the peak of the Dst index during the geomagnetic storms are plotted against the true speeds of the CMEs. The quantities are found to be weakly correlated for the selected events with a linear Pearson correlation coefficient of -0.49. As already stated, the GCS model fits the flux rope to a CME assuming conical-shaped legs joining each other at the center of the Sun. The aspect ratio (κ) parameter is the sine of the half angle (δ) of the cone ($\kappa = \sin\delta$) (Thernisien, 2011). The face-on width (ω_{FO}) of the CME can be calculated by following the formula $\omega_{FO} = 2(\alpha + \delta)$, as given by Thernisien et al. (2009). The Dst indices are plotted against the quantity ω_{FO} in the Figure 6.3b. It can be seen that the geoeffective impact of the events is quite strongly correlated with their face on widths with a linear Pearson correlation coefficient of -0.73.

As we see from the plots discussed above, the geoeffective parameters of CMEs such as the transit time and the Dst index, do not strictly correlate with any single feature of the CMEs but show weak correlation with significant scatter, this makes it a difficult task to perform forecasting of the geoeffectiveness of a CME with reasonable accuracy by using linear regression between these quantities. Hence, we turn to the ANN algorithm for better results. For the training of the ANN, we randomly split the entire dataset into two parts, the training set consists of 80% of the data set (53 events) and the testing set consists of the rest 20% of the data set (14 events). For the measure of improvement in the performance of the network throughout its training, we use the mean squared error between the predicted and the actual observed values of the geoeffective parameters (transit time and dst index from the table Table 6.1). Figure 6.4a shows the evolution of the loss function or in this case throughout the training and validation of the network for the CME transit time forecast.

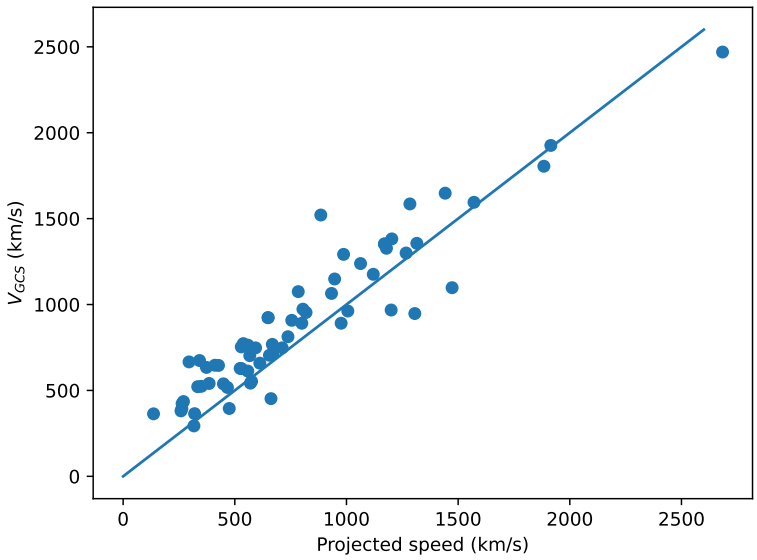

(a)

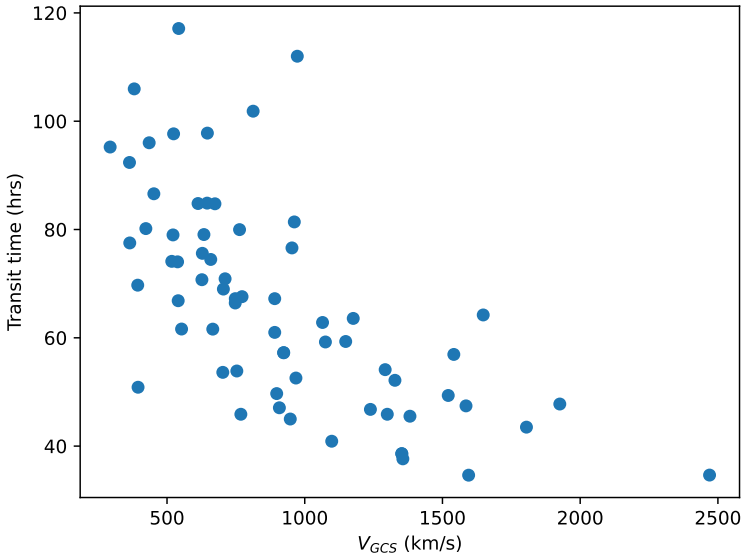

(b)

Fig. 6.2 The subplot (a) shows the calculated GCS speed (V_{GCS}) plotted against the linear projected speed obtained from the CDAW catalogue, the solid line indicates the $x = y$ line. The subplot (b) is the plot of the CME transition time or travel time from the Sun to near-Earth space against the CME speed.

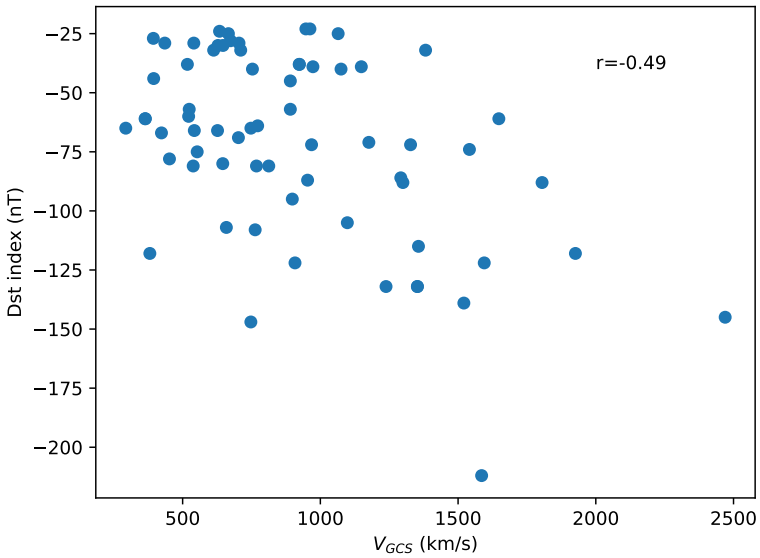

(a)

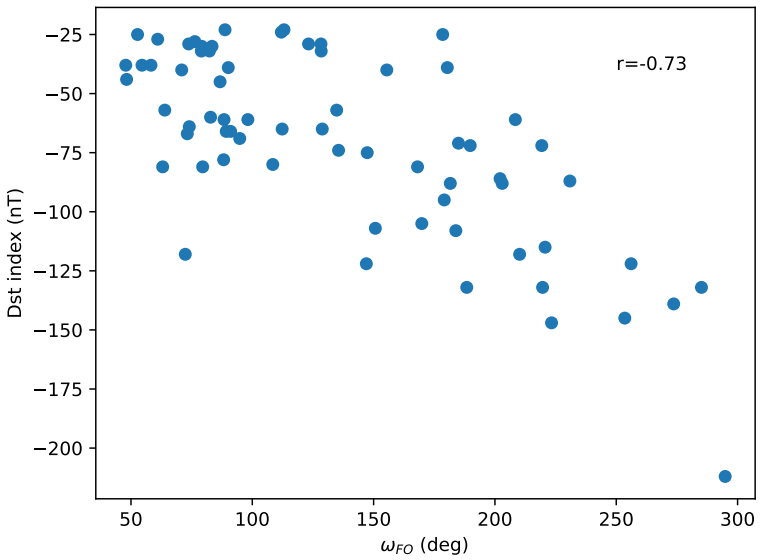

(b)

Fig. 6.3 The Dst index of the geomagnetic disturbance plotted againts (a) the GCS speed, and the (b) width of the CMEs, along with the linear Pearson correlation coefficients between the plotted quantities mentioned in the subplots.

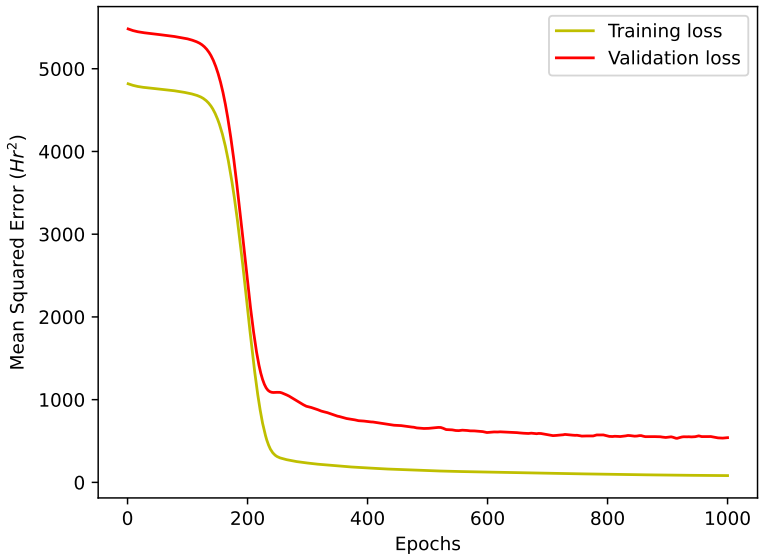

(a)

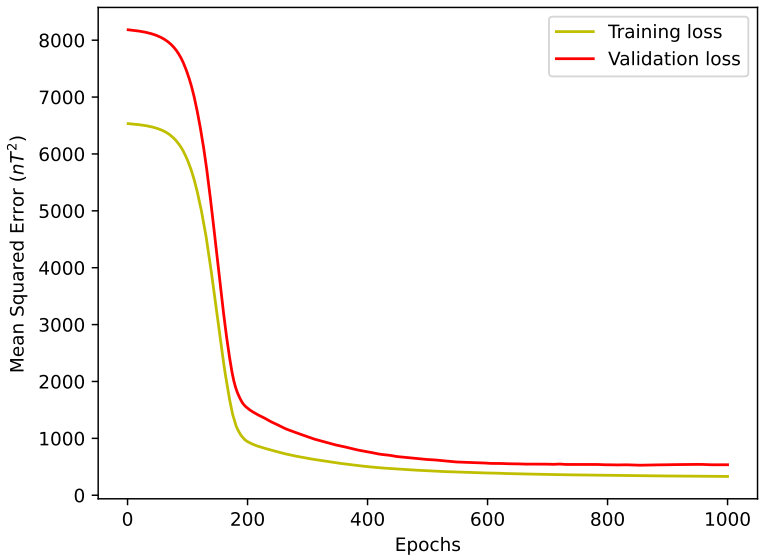

(b)

Fig. 6.4 The evolution of the training and the validation losses as measured by mean squared error throughout 1000 epochs during the training of the ANNs for forecasting (a) the CME transit time and (b)the Dst index.

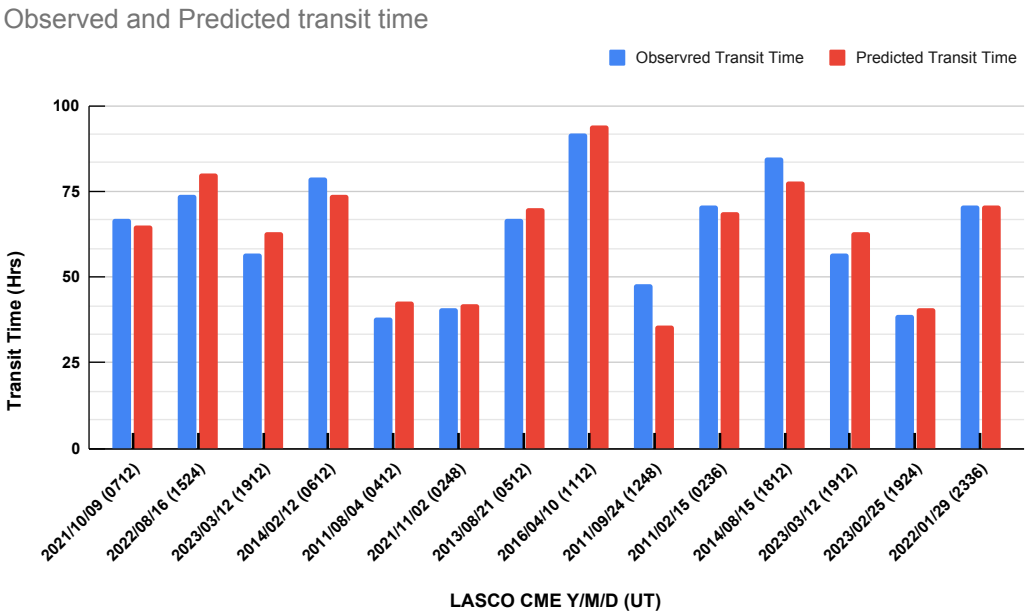

Fig. 6.5 The observed transit times of the 14 CMEs from the test set along with the transit times predicted by the ANN.

Both the training and validation loss terms start from a very high value for initial epochs as expected, and quickly drop to a much lower value where they stay stable for a sustained period of time, signaling a good and generalized training of the network. On the other hand, the Figure 6.4b shows the same for the training of the network for forecasting the Dst index. In this case also, we see a similar pattern of evolution for the loss functions indicating sufficient training of the network.

Once both the networks are trained, we deploy the trained ANNs for the prediction of transit time and Dst index for the 14 events in the testing set and to analyse the performance of the networks, we use the Mean Absolute Deviation (MAD) and the standard deviation of the absolute values of the errors as the key metric for the performance of the ANN. The Figure 6.5 shows the observed and the predicted transit times for the CMEs in the testing set. The ANN performs reasonably well in predicting the transit times for these 14 events with MAD of 4.22 hrs and a standard deviation of 2.80 hrs. The Figure 6.6 shows the

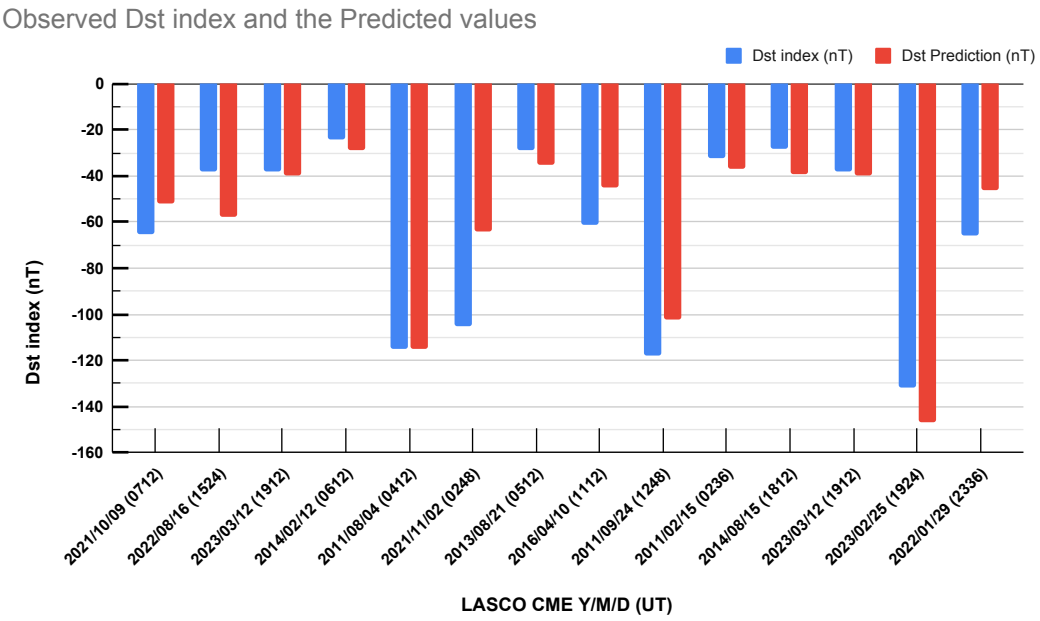

Fig. 6.6 The observed Dst indices of the geomagnetic storms caused by the 14 CME events of the test set along with the Dst indices predicted by the ANN.

observed Dst indices along with the predicted ones for the same events. In this case, the MAD of the prediction is 12.39 nT with a standard deviation of 10.28 nT.

6.4 Conclusion

In this work, we have showcased the effectiveness of the ANN algorithms aided by the forward modelling of the CMEs, in forecasting the geoeffectiveness of the CMEs. Although the datasets available for performing GCS forward modelling is limited to a small number of events due to the lack of simultaneous multi-viewpoint observations and occasional data gaps during major events, the ANN algorithms do perform reasonably well in forecasting the transit time of the CMEs with a significantly small MAD of 4.22 hrs with standard deviation of 2.80 hrs as compared to many previous studies. However, the errors in the forecast of the Dst indices are a bit larger which can be significantly improved in the

future by including the observations of the future events in the training of the algorithm. In conclusion, the initial CME parameters as obtained from the GCS model can be an excellent and reliable source for machine learning algorithms like the one employed here to understand the nature and evolution of the CMEs in the near-sun space and in forecasting the time and severity of their impact on the Earth's magnetosphere. The most beneficial aspect of forecasting capability of the geoffectiveness using the initial CME parameters is that the time window of the forecast is significantly large as the CMEs take only a small fraction of their transit time to evolve within the field of views of the instruments used in this study.